AIAA JOURNAL
Vol. 32, No. 5, May 1994

Transition Correlations in Three-Dimensional Boundary Layers

Helen L. Reed* and Timothy S. Haynes†
Arizona State University, Tempe, Arizona 85287

The stability and transition characteristics of three-dimensional boundary-layer flows are examined. First, the flow over a rotating cone is considered computationally. An increase of stagnation temperature is found to be only slightly stabilizing. Parameter studies on the simple rotating-cone geometry provide a large database of three-dimensional boundary-layer profiles and associated stability characteristics. To determine the possibility of correlating transition location with parameters based purely on basic-state three-dimensional boundary-layer profile characteristics, an empirical transition location of $N = 9$ is assumed. Transition location does not correlate with the traditional crossflow Reynolds number. A more appropriate definition for crossflow Reynolds number is found and termed $R_{cf(new)}$. This new parameter appears to correlate for transition location when plotted against maximum crossflow velocity. Then, the flow over a yawed cone is considered experimentally. The correlation results obtained from the rotating-cone work are applied to the actual measured transition locations on two different yawed-cone models under various angle-of-attack conditions in two different experimental facilities and are verified. This correlation is only suggested as a tool for preliminary transition prediction and design in three-dimensional boundary layers; once a preliminary shape is selected, further linear stability theory or parabolized stability equation calculations are strongly urged.

Nomenclature

A = $Pr^{1/2}(\gamma - 1)M_e^2/2$
C^* = Chapman-Rubesin parameter based on T^*
C^*_{ad} = Chapman-Rubesin parameter based on T^*_{ad}
H = factor in $R_{cf(new)}$ including compressibility
H_{cf} = crossflow shape factor, δ_{10}/y_{max}
h_3 = $r + y \cos\theta$ (dimensional)
L = factor in $R_{cf(new)}$ including cooling
M = freestream Mach number
M_e = local edge Mach number with respect to a reference frame fixed to surface of rotating cone
N = amplification factor
Pr = Prandtl number at reference temperature T^*
R = $R_{cf(new)}U_e/W_{max}$, Eq. (17)
R_{cf} = traditional crossflow Reynolds number, Eq. (13)
$R_{cf(new)}$ = new crossflow Reynolds number, Eq. (10)
R_t = Re at transition according to linear stability theory
R_0 = Re at x_0
Re = Reynolds number based on local edge conditions and reference boundary-layer thickness
r = distance from body axis to surface, dimensional
r = radial distance on rotating disk, dimensional
T = temperature, dimensional
T_{ad} = local adiabatic wall temperature, dimensional
T_e = edge temperature, dimensional
T_w = local wall temperature, dimensional
T^* = reference temperature, dimensional
T^*_{ad} = reference temperature for adiabatic wall, dimensional
U_e = local inviscid flow speed; for rotating cone, reference frame is fixed to the surface, dimensional
W_{max} = maximum crossflow velocity, that is, velocity in direction perpendicular to local inviscid flow; for rotating cone, reference frame is fixed to surface, dimensional
x, y, z = streamwise, normal-to-wall, spanwise coordinates, dimensional
x_0 = initial streamwise position for calculation of N; or upstream position for marching, dimensional
y_{max} = height of W_{max} above wall, dimensional
$-\alpha_I$ = negative of imaginary part of streamwise component of wave number; spatial growth rate
β_r, β_I = real, imaginary part of spanwise component of wave number
γ = edge ratio of specific heats
δ = boundary-layer thickness, dimensional
δ_{ad} = boundary-layer thickness for adiabatic wall, dimensional
δ_{cool} = boundary-layer thickness for cooled wall, dimensional
δ_{incomp} = boundary-layer thickness for incompressible constant-temperature flow, dimensional
δ_r = reference boundary-layer thickness, dimensional; $(\nu_e x/U_e)^{1/2}$
δ_{10} = height above y_{max} where crossflow is 10% W_{max}, dimensional
η = similarity variable in normal-to-wall direction; normal-to-wall computational coordinate
θ = angle between body surface and body axis
ν_e = edge kinematic viscosity, dimensional
ξ, η, ζ = streamwise, normal-to-wall, spanwise computational coordinates
Ω = cone rotational speed; rotating-disk rotational speed

Received Oct. 1, 1992; revision received Aug. 4, 1993; accepted for publication Aug. 9, 1993.

*Professor, Mechanical and Aerospace Engineering. Associate Fellow AIAA.
†Graduate Research Assistant, Mechanical and Aerospace Engineering.

I. Introduction

A. Background

AT high speeds, the wings of vehicles are swept and the flow is three dimensional. In the leading-edge region of a swept surface, both the surface and flow streamlines are highly curved. The combination of pressure gradient and sweep deflects the inviscid-flow streamlines inboard; this mechanism reoccurs in the pressure-recovery region near the trailing edge. Because of the lower momentum fluid near the wall, this deflection is made larger within the boundary layer and causes

crossflow, i.e., the development of a velocity component inside the boundary layer that is perpendicular to the local inviscid-flow velocity vector. The crossflow profile has a maximum velocity somewhere in the middle of the boundary layer, going to zero on the surface and at the boundary-layer edge. The crossflow profile exhibits an inflection point (a condition that is known to be dynamically unstable) causing so-called crossflow vortex structures to form with their axes aligned approximately in the local inviscid direction.[1] These crossflow vortices all rotate in the same direction and take on the familiar cat's-eye structure when viewed along their axes. Examples of other three-dimensional flows of practical interest include rotating cones, yawed cylinders and cones, corners, inlets, and rotating disks. It appears that a consistent characteristic of all of these flows is the presence of streamwise vorticity within the shear layer. For a recent review of this subject, see Reed and Saric.[2]

B. Transition Prediction and Correlation Parameters

The state-of-the-art transition-prediction method still involves linear stability theory coupled with an e^N transition-prediction scheme[3,4] and is applied at all speeds.[5] Linear stability theory proves useful in determining the important flow conditions or parameters affecting transition and their trends, that is, whether and by how much a change of some parameter is stabilizing or destabilizing. Here, the resultant growth or decay of small disturbances in the boundary layer which lead to transition is the measure of transition enhancement or delay. N is the result of the integration of the linear growth rate from the first neutral-stability point to a location somewhere downstream on the body. Thus, e^N is the ratio of the amplitudes at the two points, and the method correlates the transition Reynolds number with N.

Aside from the e^N method along with various modifications (e.g., Cebeci et al.[6]), several past investigators have identified nondimensional parameters (based solely on basic-state boundary-layer profiles) quantifying the characteristics of the crossflow instability and, in some cases, attempted to correlate these numbers with transition location. Some examples follow.

In subsonic flow, a crossflow Reynolds number was introduced as the governing parameter and it was suggested that transition occurs when the crossflow Reynolds number becomes equal to about 150; a value for W_{max} of order 3% of the local inviscid speed is typical for wind-tunnel and flight tests. (Poll[4] discusses the details of this correlation.) Pfenninger[7] used crossflow shape factor $H_{cf} = y_{max}/\delta_{10}$ and crossflow Reynolds number $R_{cf} = W_{max}\delta_{10}/\nu_e$ in the design of supercritical airfoils. Dagenhart[8] then considered stationary crossflow vortices and, instead of solving the linear stability equations each time, he used a table lookup of growth rates based on the profile characteristics: crossflow shape factor and crossflow Reynolds number. He reported that he could adequately reproduce the results of the more complicated stability codes using less than 2% of the computer time.

In supersonic flow, Chapman[9] and Pate[10] made similar conclusions that crossflow Reynolds number correlates well with transition location. On a yawed cone, King[11] found that there was no correlation with the traditional crossflow Reynolds number. However, when he reformulated this parameter to include both compressibility and yawed-cone geometry effects, he found a correlation for both his and Stetson's[12] data, but only as a function of azimuthal angle around the cone. Therefore, because this parameter depends on cone yaw angle, cone half-angle, and azimuthal angle, it is limited in its applicability to general geometries.

C. Objectives

With the current interest in high-speed flight, there is a keen desire to determine correlating parameters, based purely on basic-state profiles, that can be easily incorporated into existing basic-state codes and will estimate transition location (or trends) for crossflow-dominated problems. In the present work, to evaluate parameters quantifying stability characteristics, the linear stability of the flow over a rotating cone at zero incidence is examined. This simple geometry has been used successfully in incompressible flow as a model for the crossflow instability.[13,14] At very high speeds, where even the basic-state calculations are a problem, the simple geometry of the rotating cone becomes a suitable and valuable model to study the crossflow instability.[1] Results are then applied to available experimental data on other geometries.

II. Numerical Approach

A sharp cone rotating about its axis located in a supersonic freestream at zero angle of attack is considered, see Fig. 1. The governing boundary-layer equations for a compressible ideal-gas flow are solved in a body-oriented coordinate system using the Cebeci-Keller box scheme.[15] By varying the freestream Mach number, rotational speed, cone angle, and position on the cone, a wide parameter range of possible three-dimensional boundary layers can be studied, and the various nondimensional parameters associated with the crossflow profile are easily fixed (Re, R_{cf}, H_{cf}, . . .). The details of the basic-state formulation are available in Ref. 1.

The stability of this laminar boundary layer is determined using linear theory, with the stability equations solved to determine the eigenvalues using the compact two-point, fourth-order finite-difference method.[16] The details of the linear stability analysis are also available in Ref. 1.

Locally, for a given frequency, the maximum growth rate $-\alpha_I$ is found by varying β_r and setting $\beta_I = 0$. Then, the amplification factor N is determined by integrating the growth rate in the streamwise direction x from the branch I location x_0. With the Reynolds numbers (based on reference boundary-layer thickness δ_r) at x_0 and x being $R_0 = (U_e x_0/\nu_e)^{1/2}$ and

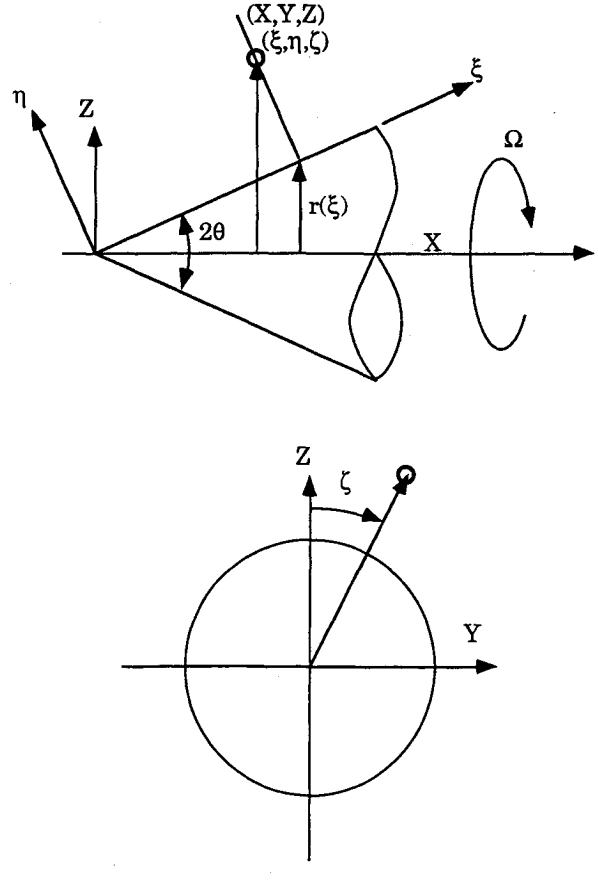

Fig. 1 Rotating cone in supersonic axial flow and coordinate system.

$Re = (U_e x/\nu_e)^{1/2}$, respectively, and the growth rate $-\alpha_I$ nondimensional with respect to δ_r

$$N = -2\int_{R_0}^{Re} \alpha_I \, d(Re) \tag{1}$$

To estimate transition location for the present study, a value of $N = 9$ is empirically chosen because values of 9–10 have been demonstrated to apply over a large speed range for various flow conditions.[5] Then, all possible frequencies are sampled to determine where each individual disturbance achieves $N = 9$. The most upstream of this locus of streamwise locations is deemed the estimated transition location. The values of other parameters characterizing crossflow may then be evaluated against the results of $N = 9$. It must be emphasized that the purpose of this empirical computational study is to reveal any trends, and the results are later applied to and verified by experimental measurements.

III. New Crossflow Reynolds Number

The object of the present work is to investigate parameters, based purely on basic-state profiles, that will estimate transition location (or trends) for crossflow dominated problems. As pointed out in the Introduction, the traditional crossflow Reynolds number is successfully used for low-speed flows. In this section, an attempt is made to compensate for compressibility effects and to adjust this parameter accordingly.

White[17] points out that to estimate the boundary-layer thickness for a flat plate, one should consider the similarity variable so that

$$\delta Re/x = \int_0^{\eta(\delta)} (T/T_e) \, d\eta \tag{2}$$

(Refs. 18–20). Taking advantage of this idea, then, a three-dimensional compressible boundary layer δ should approximately thicken with respect to the corresponding "incompressible" layer δ_{incomp} as

$$\frac{\delta}{\delta_{incomp}} = \eta(\delta)^{-1} \int_0^{\eta(\delta)} (T/T_e) \, d\eta \tag{3}$$

The quantity δ_{incomp} is a constant-temperature incompressible value that is determined simply by setting T/T_e everywhere equal to unity in Eq. (2); that is, $\delta_{incomp} Re/x = \eta(\delta)$.

In addition, the estimated thickness of a cooled-wall boundary layer δ_{cool} to that of an adiabatic wall δ_{ad} can be estimated as (following suggestions of White[17] and considering a Crocco[21]-Busemann[22] relationship between velocity and temperature, with a recovery factor included for Prandtl number effects[23] and quantities evaluated at the reference temperature[24])

$$\delta_{cool}/\delta_{ad} = (C^*/C^*_{ad})^{1/2} (3.279 + 1.721[T_w/T_{ad}][1 + A] + 0.664A)/(5 + 2.385A) \tag{4}$$

where

$$A = Pr^{1/2}(\gamma - 1)M_e^2/2 \tag{5}$$

$$C^* = (T^*/T_e)^{1/2}(1 + 110.4/T_e)/([T^*/T_e] + 110.4/T_e) \tag{6}$$

$$C^*_{ad} = (T^*_{ad}/T_e)^{1/2}(1 + 110.4/T_e)([T^*_{ad}/T_e] + 110.4/T_e) \tag{7}$$

$$T^*/T_e = 0.5 + 0.5T_w/T_e + A/6 \tag{8}$$

$$T^*_{ad}/T_e = 0.5 + 0.5(1 + A) + A/6 \tag{9}$$

where the Chapman-Rubesin[25] parameter is approximated as a constant C^* across the boundary layer.

Now the "boundary-layer thickness" present in the crossflow Reynolds number is δ_{10}, and so δ is replaced with δ_{10} in Eq. (3). Because the incompressible crossflow Reynolds number correlates reasonably well for incompressible flows, a new general definition for R_{cf}, then, is

$$R_{cf(new)} = HLR_{cf} = HLW_{max}\delta_{10}/\nu_e \tag{10}$$

where

$$H = \eta(\delta_{10}) \Big/ \int_0^{\eta(\delta_{10})} (T/T_e) \, d\eta \tag{11}$$

$$L = (C^*/C^*_{ad})^{1/2}(3.279 + 1.721[T_w/T_{ad}][1 + A] + 0.664A)/(5 + 2.385A) \tag{12}$$

and all temperatures are in Kelvin and $\eta(\delta_{10})$ is the value of η at δ_{10}. The quantity δ_{10} has been scaled back to an incompressible value with the inclusion of the new factor H. To compensate for a cooled wall, then, the factor L is used. Note that, because one is essentially taking the ratio of two normal-to-the-wall lengths, the new factor H is easily computed no matter how the normal-to-the-wall coordinate η is defined. Note also that $R_{cf(new)}$ reduces to R_{cf} for incompressible, adiabatic-wall flows.

IV. Results

A. Rotating-Cone Calculations

Using the traditional crossflow Reynolds number and shape factor

$$R_{cf} = W_{max}\delta_{10}/\nu_e \tag{13}$$

$$H_{cf} = y_{max}/\delta_{10} \tag{14}$$

Figure 2 shows the attempt at transition correlations for the present rotating-cone calculations at a freestream Mach number of $M = 3$ and various cone angles θ, rotational speeds Ω, and wall and freestream temperatures T_w and T_e, respectively. The various flow conditions represented are documented in Table 1. The spread in R_{cf} is on the order of 200% with values ranging from 250–450 and is therefore not useful

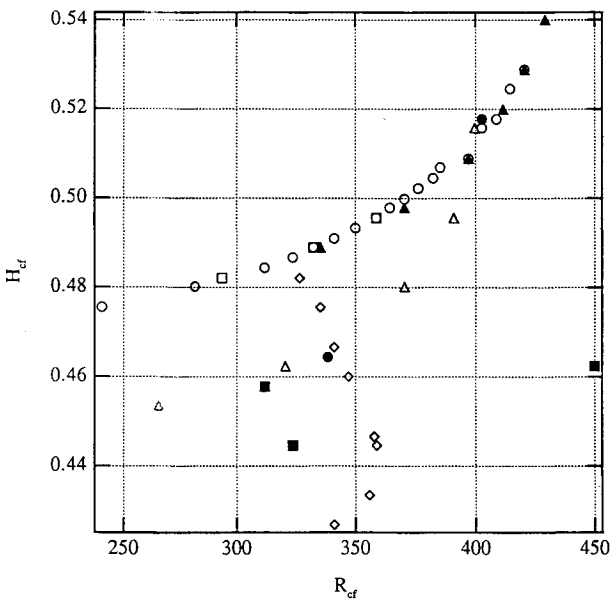

Fig. 2 Traditional crossflow Reynolds number vs shape factor at transition ($N = 9$) for various wall- and freestream-temperature conditions at $M = 3$: ▲ set I, □ set II, ○ set III, △ set IV, ● set V, ◇ set VI, and ■ set VII.

Table 1 Rotating-cone configurations for $M = 3$

Set	Fixed parameters	Varied parameters and range
I	$\Omega = 0.375$ $T_e = 70$ K Adiabatic wall	θ, deg 10–35
II	$\Omega = 0.25$ $T_e = 70$ K Adiabatic wall	θ, deg 10–20
III	$\theta = 15$ deg $T_e = 70$ K Adiabatic wall	Ω 0.1–0.8
IV	$\theta = 15$ deg $T_e = 260$ K Adiabatic wall	Ω 0.1–0.8
V	$\Omega = 0.375$ $T_e = 260$ K Adiabatic wall	θ, deg 10–35
VI	$\theta = 15$ deg $T_e = 70$ K Cooled wall	Ω 0.1–0.8
VII	$\theta = 15$ deg $T_e = 260$ K Cooled wall	Ω 0.4–0.8

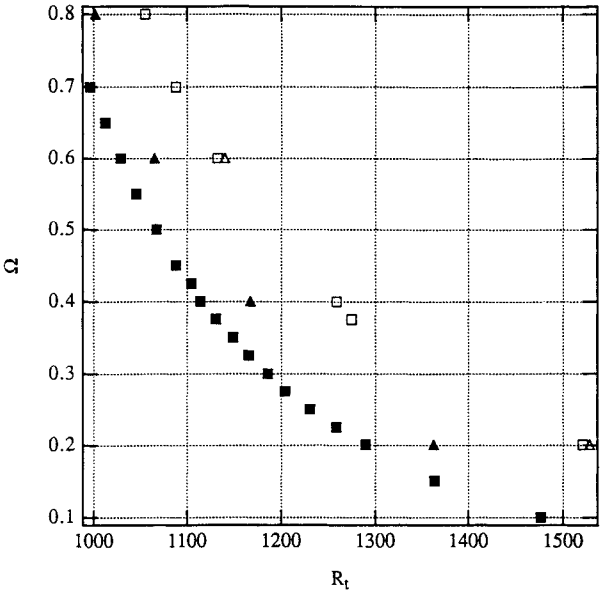

Fig. 3 Transition Reynolds number ($N = 9$) vs cone rotational speed for various wall- and freestream-temperature conditions at $M = 3$: ■ $T_e = 70$ K, adiabatic; □ $T_e = 70$ K, $T_w/T_{ad} = 0.6$; ▲ $T_e = 260$ K, adiabatic; and △ $T_e = 260$ K, $T_w/T_{ad} = 0.6$.

for design. Moreover, these values differ a great deal from those on the order of 150 reported for low-speed flows. Figure 3 shows the same data plotted considering transition Reynolds number R_t vs rotational speed Ω (with increasing Ω implying increasing three-dimensional effects). Cooling is only slightly stabilizing (see also Refs. 1, 26–28), and an increase of stagnation temperature has an even smaller stabilizing effect. Even so, these temperature effects produce large changes in R_{cf}.

Table 2 shows comparative results for upstream freestream Mach numbers of $M = 0.01$ and $M = 3$ for different freestream-temperature (T_e) and surface-temperature (T_w/T_e) conditions and a wide variety of rotating-cone geometries. The $M = 3$ conditions correspond to those in Fig. 2 and Table 1. The results of the new definition for crossflow Reynolds number with compressibility effects included, $R_{cf(new)}$ [Eq. (10)], are contrasted with those obtained from the traditional definition, R_{cf} [Eq. (13)]. Also included is the maximum crossflow velocity; the significance of this should become apparent in the subsequent discussion.

Table 2 Traditional and new crossflow Reynolds numbers for rotating-cone configurations

M	M_e	T_e, K	T_w/T_e	R_{cf}	$R_{cf(new)}$	W_{max}/U_e, %
0.01	0.01	300	1	165	165	5.9
3	3.1	70	2.6	241	119	3.2
3	3.2	70	2.7	311	149	4.5
3	3.4	70	2.9	373	170	5.7
3	3.6	70	3.2	409	175	6.1
3	3.8	70	3.5	428	171	6.1
3	3.1	260	2.5	210	107	2.6
3	3.1	260	2.6	263	132	3.6
3	3.2	260	2.7	316	154	4.8
3	3.4	260	2.9	366	168	5.9
3	3.7	260	3.2	388	166	6.1
3	3.9	260	3.5	400	161	6.0
3	3.2	70	1.5	339	177	4.6
3	3.3	70	1.5	354	179	5.5
3	3.6	70	1.5	354	168	6.1
3	3.8	70	1.5	344	155	6.1
3	4.1	70	1.5	332	140	5.8
3	4.2	260	1.5	448	201	5.6
3	3.8	260	1.5	323	156	6.0
3	4.1	260	1.5	310	142	5.7

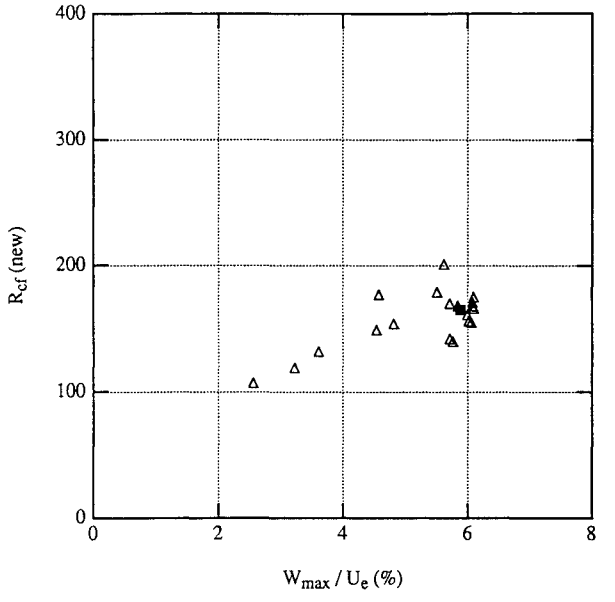

Fig. 4 New definition of crossflow Reynolds number (including compressibility effects) vs maximum crossflow velocity for computational rotating-cone data assuming a transition location of $N = 9$: various freestream- and wall-temperature conditions as well as cone geometries are represented; △ $M = 3$ and ■ $M = 0$.

The new crossflow Reynolds number, Eq. (10), is shown plotted vs maximum crossflow velocity in Fig. 4. Included are the values for all of the various rotating-cone configurations listed in Table 2 at both $M = 0.01$ and $M = 3$. Two observations can be made at this point. 1) There appears to be a relationship between $R_{cf(new)}$ and W_{max}. 2) The computed incompressible value (for $M = 0.01$) now falls among the new compressible values of crossflow Reynolds number (for $M = 3$).

B. Yawed-Cone Experiments

Because linear stability theory with $N = 9$ applied to a rotating cone was used to find these trends, it is important to verify them against experimental data. The three-dimensional transition data of King[11] on the yawed cone in the Mach 3.5 quiet tunnel at NASA/Langley was a good candidate for this validation. The King experiment was on a 5-deg half-angle cone yawed at 0.6, 2, and 4 deg. The data of transition locations for various freestream conditions, both quiet and noisy, are documented in Ref. 11.

King provided the present authors with the computational mean-flow profiles he used in the analysis of his experimental results. In the experiment, tunnel conditions were varied until transition was achieved in turn at each of the cone azimuthal angles of 0 (windward), 30, 60, 90, 120, 150, and 180 deg (leeward). This method of varying transition location corresponded to changing the unit Reynolds number and it must be assumed that there are no unit Reynolds-number effects. Then the velocity and temperature profiles were computer generated for the experimentally determined transition conditions at each location. King[11] points out that, because of the considerable growth of the boundary layer with increasing azimuthal angle, the boundary-layer assumptions break down

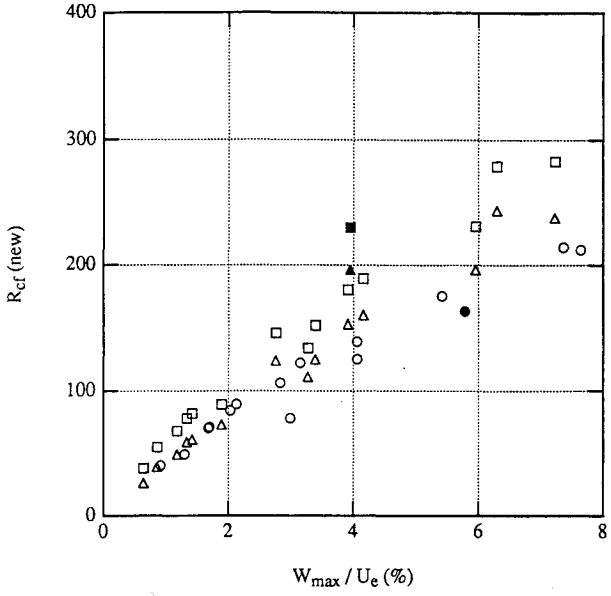

Fig. 5 New definition of crossflow Reynolds number (including compressibility effects) vs maximum crossflow velocity for experimental yawed-cone data of King[11] at M = 3.5 and Stetson[12] at M = 5.9: open symbols are for azimuthal angles 30, 60, 90, and 120 deg; filled symbols are for azimuthal angle 150 deg; □ ■ King quiet, △ ▲ King noisy, and ○ ● Stetson.

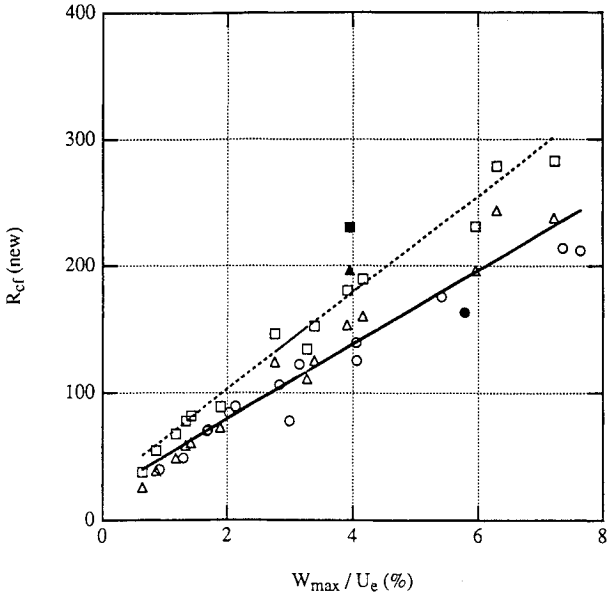

Fig. 6 Linear least-squares fit of the experimental yawed-cone data of King[11] at M = 3.5 and Stetson[12] at M = 5.9: open symbols are for azimuthal angles 30, 60, 90, and 120 deg; filled symbols are for azimuthal angle 150 deg; □ ■ King quiet, △ ▲ King noisy, and ○ ● Stetson; --- quiet fit, $R_{cf(new)} = (38.0)W_{max}/U_e + 26.7$ and ——— noisy fit, $R_{cf(new)} = (29.1)W_{max}/U_e + 21.5$.

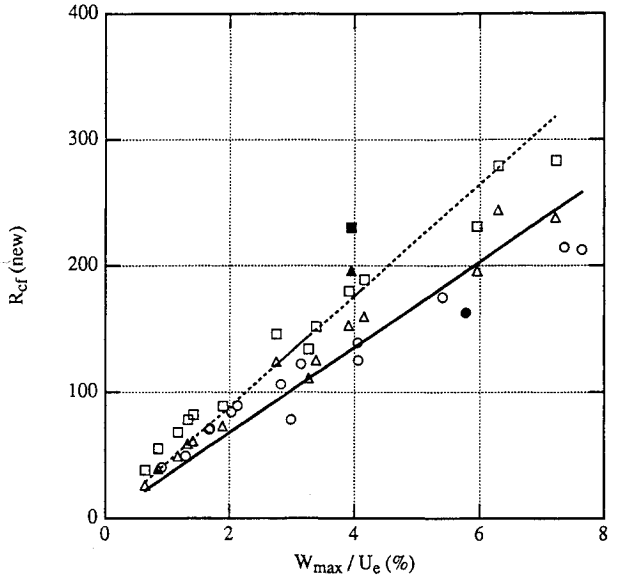

Fig. 7 Linear least-squares fit through the origin of the experimental yawed-cone data of King[11] at M = 3.5 and Stetson[12] at M = 5.9: open symbols are for azimuthal angles 30, 60, 90, and 120 deg; filled symbols are for azimuthal angle 150 deg; □ ■ King quiet, △ ▲ King noisy, and ○ ● Stetson; --- quiet fit, $R_{cf(new)} = (44.0)W_{max}/U_e$ and ——— noisy fit, $R_{cf(new)} = (33.7)W_{max}/U_e$.

near the leeward ray and the code was unable to obtain solutions for azimuthal angle greater than 144 deg for the largest angle of attack, 4 deg, and thus extrapolation had to be used. Therefore, in all calculations presented here (Figs. 5–7), azimuthal angle 150 deg results for an angle of attack of 4 deg are indicated with a filled-in symbol.

Applying the traditional crossflow Reynolds number, Eq. (13), to the computer-generated profiles for King's experiments gives values ranging from 80 to 640 for quiet conditions and from 60 to 560 for noisy conditions. Once again, these results indicate too much of a spread for design, and the values are inconsistent with low-speed results. Applying the new crossflow Reynolds number, Eq. (10), on the other hand, to these same profiles and plotting the results for azimuthal angles of 30, 60, 90, 120, and 150 deg for all three angles of attack and both quiet- and noisy-freestream conditions gives Fig. 5. This is discussed subsequently.

King[11] also considered the M = 5.9 experiments of Stetson[12] on an 8-deg half-angle cone yawed at 1, 2, and 4 deg and again provided the present authors with the mean-flow profiles he used in the evaluation of this experiment. Considering what Stetson[12] terms as the beginning of transition and applying Eq. (13) gives values ranging from 140 to 780. The results, then, of applying the new crossflow Reynolds number, Eq. (10), to these profiles and plotting the results for azimuthal angles of 30, 60, 90, 120, and 150 deg for all three angles of attack are also found in Fig. 5. Once again, because the same computer code was used to generate the mean-flow profiles as was used for the King experiments, azimuthal angle 150 deg results for an angle of attack of 4 deg are indicated with a filled-in symbol. The surface of Stetson's cone was cooled, whereas the wall of King's cone was adiabatic. The Stetson data were taken with a noisy freestream, and it is surprising that the Stetson data agrees so well with the King noisy data considering that two different facilities are involved with different flowfield conditions and characteristics.

The trends of the three sets of experimental data in Fig. 5 suggest a linear least-squares fit for the correlation of $R_{cf(new)}$ and W_{max}.

Quiet (M = 3.5)

$$R_{cf(new)} = 26.7 + 38.0W_{max}/U_e \qquad (15)$$

for $2\% < W_{max}/U_e < 8\%$.

Noisy ($M = 3.5$ and $M = 5.9$)

$$R_{cf(new)} = 21.5 + 29.1 W_{max}/U_e \quad (16)$$

for $2\% < W_{max}/U_e < 8\%$ where W_{max}/U_e is in percent. The two curves are included with the data in Fig. 6. Below the curves, the flow has not undergone transition. At this point, it is not clear what happens when W_{max}/U_e is greater than 8%, and caution is urged in extrapolation. (Figure 3 indicates that transition location becomes less sensitive as rotation speed increases, so that large departures from the indicated values of W_{max}/U_e may result in different local behavior of the correlation curve.) Moreover, the lower end of the curve is also suspect since crossflow has been observed in low-speed flows to appear when crossflow Reynolds number is order 100. Below this value, Tollmien-Schlichting instability should be dominant.

From visual inspection, the data in Fig. 5 (in the range from $2\% < W_{max}/U_e < 8\%$) could also be approximated by a line that passes through the origin. Assuming a least-squares straight line fit through the origin, then, the implication is that the correlation reduces to

$$\begin{aligned} R &= R_{cf(new)} U_e/W_{max} \\ &= HL\delta_{10} U_e/\nu_e \\ &= 44.0 \text{ (quiet)} \\ &= 33.7 \text{ (noisy)} \end{aligned} \quad (17)$$

for $2\% < W_{max}/U_e < 8\%$ at transition, and W_{max} drops out of consideration (Fig. 7). In other words, a universal constant R is suggested, based on available theoretical and experimental data, for transition prediction and evaluation in three-dimensional boundary layers. Again the range of validity should be considered, $2\% < W_{max}/U_e < 8\%$. For example, W_{max}/U_e for the rotating disk is approximately 18% and with $R = 44$ [from Eq. (17)], the disk Reynolds number at transition is predicted to be $r(\Omega/\nu_e)^{1/2} = 10$ which is way too low from the observed value of order 500 (Refs. 29 and 30).

V. Conclusions

For the examination of three-dimensional effects in high-speed flows, a rotating cone is used. A large parameter range of flow conditions can be studied and trends observed, which are then verified by the available experiments. The following conclusions can be drawn from this study.

1) Considering a perfect gas, increasing freestream stagnation temperature only slightly stabilizes the crossflow instability. This is in contrast to two-dimensional basic states where a large effect on Tollmien-Schlichting instability is observed.[31]

2) For the rotating cone, transition location ($N = 9$) does not correlate with the traditional crossflow Reynolds number.

3) When compressibility and cooling effects are included for both the rotating cone and the yawed cone, a new crossflow Reynolds number $R_{cf(new)}$ is found. The values of $R_{cf(new)}$ for W_{max}/U_e order 3% are now in the neighborhood of 150 consistent with the low-speed values reported. This new parameter contains no geometry explicitly and applies for gas flows with Prandtl number different from unity. It reduces to the traditional crossflow Reynolds number when Mach number goes to zero.

4) A relationship exists between the new crossflow Reynolds number and the maximum crossflow velocity at transition. This result has been verified for the theoretical rotating-cone data and the experimental yawed-cone data of both King[11] and Stetson.[12]

5) From this relationship, a new universal parameter R is suggested that can be calculated solely from the basic-state profiles. As with $R_{cf(new)}$, this parameter also contains no geometry explicitly and applies for gas flows with Prandtl number different from unity. As such, it can aid in preliminary transition prediction and design, including the evaluation of parameter trends, for three-dimensional boundary layers. Once a preliminary shape is selected, further linear stability theory or parabolized stability equation calculations are strongly urged.

6) The reader is reminded to exercise caution in using a correlation beyond its database. To reiterate, rotating-cone and yawed-cone geometries were considered and the range of the data is $2\% < W_{max}/U_e < 8\%$.

Acknowledgments

This work was supported at various stages by the Air Force Office of Scientific Research under Contract F49620-88-C-0076, the National Science Foundation under the Presidential Young Investigator Award, McDonnell/Douglas in St. Louis, and General Dynamics/Fort Worth and is currently supported by NASA/Ames Research Center under the Graduate Student Researchers Program and the National Science Foundation under the Faculty Awards for Women in Science and Engineering Program. The first author acknowledges her support by the Institute of Fluid Science, Tohoku University, Sendai, Japan, while on sabbatical there.

The first author especially thanks Rudy King and Dennis Bushnell of NASA/Langley Research Center for supplying the basic-state profiles for the yawed-cone experiments of both King and Stetson.

References

[1]Balakumar, P., and Reed, H. L., "Stability of Three-Dimensional Supersonic Boundary Layers," *Physics of Fluids A*, Vol. 3, No. 4, 1991, pp. 617–632.

[2]Reed, H. L., and Saric, W. S., "Stability of Three-Dimensional Boundary Layers," *Annual Review of Fluid Mechanics*, Vol. 21, Jan. 1989, pp. 235–284.

[3]Mack, L. M., "Boundary-Layer Linear Stability Theory," Special Course: Stability and Transition of Laminar Flows, AGARD-709, March 1984.

[4]Poll, D. I. A., "Transition Description and Prediction in Three-Dimensional Flows," Special Course: Stability and Transition of Laminar Flows, AGARD-709, March 1984.

[5]Bushnell, D. M., Malik, M. R., and Harvey, W. D., "Transition Prediction in External Flows via Linear Stability Theory," *IUTAM Symposium Transsonicum III*, edited by J. Zierep and H. Oertel, Springer-Verlag, Berlin, 1989.

[6]Cebeci, T., Chen, H. H., and Arnal, D., "A Three Dimensional Linear Stability Approach to Transition on Wings at Incidence," *Fluid Dynamics of Three-Dimensional Turbulent Shear Flows and Transition*, AGARD-CP-438, Oct. 1988.

[7]Pfenninger, W., "Laminar Flow Control Laminarization," Special Course: Concepts in Drag Reduction, AGARD-R-654, March 1977.

[8]Dagenhart, J. R., "Amplified Crossflow Disturbances in the Laminar Boundary Layer on Swept Wings with Suction," NASA TP 1902, Nov. 1981.

[9]Chapman, G. T., "Some Effects of Leading Edge Sweep on Boundary-Layer Transition at Supersonic Speeds," NASA TM D-1075, 1961.

[10]Pate, S. R., "Dominance of Radiated Aerodynamic Noise on Boundary-Layer Transition in Supersonic-Hypersonic Wind Tunnels—Theory and Application," Arnold Engineering Development Center, TR-77-107, March 1978.

[11]King, R. A., "Mach 3.5 Boundary-Layer Transition on a Cone at Angle of Attack," AIAA Paper 91-1804, June 1991.

[12]Stetson, K. F., "Mach 6 Experiments of Transition on a Cone at Angle of Attack," *Journal of Spacecraft and Rockets*, Vol. 19, No. 5, 1982, pp. 397–403.

[13]Kobayashi, R., and Izumi, H., "Boundary-Layer Transition on a Rotating Cone in Still Fluid," *Journal of Fluid Mechanics*, Vol. 127, Feb. 1983, pp. 353–364.

[14]Kobayashi, R., Kohama, Y., and Kurosawa, M., "Boundary-Layer Transition on a Rotating Cone in Axial Flow," *Journal of Fluid Mechanics*, Vol. 127, Feb. 1983, pp. 341–352.

[15]Cebeci, T., and Bradshaw, P., *Physical and Computational As-*

pects of Convective Heat Transfer, Springer-Verlag, New York, 1984, pp. 406–415.

[16]Malik, M. R., Chuang, S., and Hussaini, M. Y., "Accurate Numerical Solution of Compressible, Linear Stability Equations," *Journal of Applied Mathematics and Physics*, Vol. 33, March 1982, pp. 189–201.

[17]White, F. M., *Viscous Fluid Flow*, McGraw-Hill, New York, 1974, pp. 591–592.

[18]Howarth, L., "Concerning the Effect of Compressibility on Laminar Boundary Layers and Their Separation," *Proceedings of the Royal Society of London A*, Vol. 194, 1948, pp. 16–42.

[19]Illingworth, C. R., "Steady Flow in the Laminar Boundary Layer of a Gas," *Proceedings of the Royal Society of London A*, Vol. 199, 1949, pp. 533–558.

[20]Stewartson, K., "Correlated Compressible and Incompressible Boundary Layers," *Proceedings of the Royal Society of London A*, Vol. 200, 1949, pp. 84–100.

[21]Crocco, L., "Sulla trasmissione del calore da una lamina piana a un fluido scorrente ad alta velocità," *L'Aerotechnica*, Vol. 12, A32, pp. 181–197.

[22]Busemann, A., *Handbuch der Physik*, Vol. 1, Pt. 1, Akademische Verlagsgesellschaft Experimentalischen, Geest and Portig, Leipzig, Germany, 1931, p. 366.

[23]Bushnell, D. M., Johnson, C. B., Harvey, W. D., and Feller, W. V., "Comparison of Prediction Methods and Studies of Relaxation in Hypersonic Turbulent Nozzle-Wall Boundary Layers," NASA TN D-5433, 1969.

[24]Dorrance, W. H., *Viscous Hypersonic Flow*, McGraw-Hill, New York, 1962, pp. 134–143.

[25]Chapman, D. R., and Rubesin, M. W., "Temperature and Velocity Profiles in the Compressible Laminar Boundary Layer with Arbitrary Distribution of Surface Temperature," *Journal of the Aeronautical Science*, Vol. 16, Sept. 1949, pp. 547–565.

[26]Lekoudis, S. G., "Stability of the Boundary Layer on a Swept Wing with Wall Cooling," *AIAA Journal*, Vol. 18, No. 9, 1980, pp. 1029–1035.

[27]Mack, L. M., "On the Stabilization of Three-Dimensional Boundary Layers by Suction and Cooling," *Laminar-Turbulent Transition*, edited by R. Eppler and H. Fasel, Springer-Verlag, Berlin, 1980, pp. 223–238.

[28]Bushnell, D. M., and Malik, M. R., "Supersonic Laminar Flow Control," NASA CP-2487, Pt. 3, March 1987, pp. 923–946.

[29]Gregory, N., Stuart, J. T., and Walker, W. S., "On the Stability of Three-Dimensional Boundary Layers with Application to the Flow due to the Rotating Disk," *Philosophical Transactions of the Royal Society of London A*, Vol. 248, 1955, pp. 155–199.

[30]Wilkinson, S. P., and Malik, M. R., "Stability Experiments in the Flow over a Rotating Disk," *AIAA Journal*, Vol. 23, No. 4, 1985, pp. 588–595.

[31]Mack, L. M., "Stability of Axisymmetric Boundary Layers on Sharp Cones at Hypersonic Mach Numbers," AIAA Paper 87-1413, June 1987.